NASA TECHNICAL NOTE

NASA TN D-8487

EMISSIONS AND TOTAL ENERGY CONSUMPTION OF A MULTICYLINDER PISTON ENGINE RUNNING ON GASOLINE AND A HYDROGEN-GASOLINE MIXTURE

John F. Cassidy

Lewis Research Center
Cleveland, Ohio 44135

NATIONAL AERONAUTICS AND SPACE ADMINISTRATION • WASHINGTON, D. C. • MAY 1977

1. Report No. NASA TN D-8487	2. Government Accession No.	3. Recipient's Catalog No.
4. Title and Subtitle EMISSIONS AND TOTAL ENERGY CONSUMPTION OF A MULTICYLINDER PISTON ENGINE RUNNING ON GASOLINE AND A HYDROGEN-GASOLINE MIXTURE		5. Report Date May 1977 6. Performing Organization Code
7. Author(s) John F. Cassidy		8. Performing Organization Report No. E-9105
9. Performing Organization Name and Address Lewis Research Center National Aeronautics and Space Administration Cleveland, Ohio 44135		10. Work Unit No. 505-05 11. Contract or Grant No.
12. Sponsoring Agency Name and Address National Aeronautics and Space Administration Washington, D. C. 20546		13. Type of Report and Period Covered Technical Note 14. Sponsoring Agency Code

15. Supplementary Notes

16. Abstract

An experimental program using a multicylinder reciprocating engine was performed to extend the efficient lean operating range of gasoline by adding hydrogen. Both bottled hydrogen and hydrogen produced by a research methanol steam reformer were used. These results were compared with results for all gasoline. A high-compression-ratio, 7.4-liter (472-in.^{3}) displacement production engine was used. Apparent flame speed was used to describe the differences in emissions and performance. Therefore, engine emissions and performance, including apparent flame speed and energy lost to the cooling system and the exhaust gas, were measured over a range of equivalence ratios for each fuel. The results were used to explain the advantages of adding hydrogen to gasoline as a method of extending the lean operating range. The minimum-energy-consumption equivalence ratio was extended to leaner conditions by adding hydrogen, although the minimum energy consumption did not change. All emission levels decreased at the leaner conditions. Also, adding hydrogen significantly increased flame speed over all equivalence ratios. Engine performance and emissions with hydrogen from the methanol reformer were about the same as those with bottled hydrogen.

17. Key Words (Suggested by Author(s))
Engines
Fuel consumption
Emission
Hydrogen

18. Distribution Statement
Unclassified - unlimited
STAR Category 07

19. Security Classif. (of this report)	20. Security Classif. (of this page)	21. No. of Pages	22. Price*
Unclassified	Unclassified	36	A03

* For sale by the National Technical Information Service, Springfield, Virginia 22161

EMISSIONS AND TOTAL ENERGY CONSUMPTION OF A MULTICYLINDER PISTON ENGINE RUNNING ON GASOLINE AND A HYDROGEN-GASOLINE MIXTURE

by John F. Cassidy

Lewis Research Center

SUMMARY

An experimental program using a multicylinder reciprocating engine was performed to extend the efficient lean operating range of gasoline by adding hydrogen. Both bottled hydrogen and hydrogen produced by a research methanol steam reformer were used. These results were compared with results for all gasoline. A high-compression-ratio, 7.4-liter (472-in.^{3}) displacement production engine was used. Apparent flame speed was used to describe the differences in emissions and performance. Therefore, engine emissions and performance, including apparent flame speed and energy loss to the cooling system and the exhaust gas, were measured over a range of equivalence ratios for each fuel.

The results were used to explain the advantages of adding hydrogen to gasoline as a method of extending the lean operating range. The minimum-energy-consumption equivalence ratio was extended to leaner conditions by adding hydrogen, although the minimum energy consumption did not change. All emission levels decreased at the leaner conditions. Also, hydrogen addition significantly increased flame speed over all equivalence ratios. Engine performance and emissions with hydrogen from the methanol reformer were about the same as those with bottled hydrogen.

INTRODUCTION

Increasing the efficiency of reciprocating engines has constantly been pursued since Otto-cycle engines were first used as vehicle powerplants. The important effects of fuel consumption on factors such as vehicle range, operating cost, and vehicle structures have always been important design considerations. During the past decade, the impact of environmental factors and a national interest in energy conservation have accentuated the need to produce clean and efficient engines. Many concepts for improving efficiency and meeting emissions standards have been tested and reported in the

literature; these ideas include using lean mixture ratios, stratified charges, and improved mixture distribution.

Lean-mixture-ratio combustion in internal-combustion engines has the potential of producing low emissions and higher thermal efficiency for several reasons. First, excess oxygen in the charge further oxidizes unburned hydrocarbons and carbon monoxide. Second, excess oxygen lowers the peak combustion temperatures, which inhibits the formation of oxides of nitrogen. Third, the lower combustion temperatures increase the mixture specific heat ratio by decreasing the net dissociation losses. Fourth, as the specific heat ratio increases, the cycle thermal efficiency also increases, which gives the potential for better fuel economy.

Efficient lean-mixture-ratio operation, in terms of good vehicle performance, fuel economy, and low hydrocarbon emissions, is limited for several reasons. A reduction in indicated mean effective pressure (IMEP) occurs with lean mixtures (refs. 1 and 2). Also, at ultralean mixture ratios, the cycle-to-cycle and cylinder-to-cylinder variations in IMEP are drastically increased, which produces sizable power fluctuations and causes engine surge and power train vibrations. Current explanations for these variations are flow velocity perturbations at the spark plug and spatial variations of turbulence in the combustion chamber. These conditions control the rate of the combustion process; therefore, lean-mixture-ratio operation involves cycle-to-cycle and cylinder-to-cylinder variations in flame speed. In addition, as the mixture ratio is made leaner, the combustion process slows and occurs over larger crank-angle intervals, thereby causing hydrocarbon emission levels and fuel consumption to rise. Also, the thermal boundary layer, or quenching distance, increases with leaner mixture ratios, which also causes hydrocarbon emission levels to rise (refs. 3 and 4). Even though excess oxygen is available to oxidize these hydrocarbons, the quenching effect of the cylinder wall will still produce a net increase in hydrocarbon emissions. Another problem is the lean-mixture-ratio misfire limit, which occurs near the flammability limits of the fuel. Cycle-to-cycle and cylinder-to-cylinder variations can cause an individual cylinder to exceed the lean flammability limits and thus misfire. Incipient lean-limit misfire is characterized by high hydrocarbon emissions, rough engine operation, and poor fuel economy.

A review of the literature dealing with the problems of lean-mixture-ratio operation shows that a fuel with a low lean flammability limit and a high flame speed might yield low exhaust emissions at ultralean conditions. Hydrogen was identified in reference 5 as having those properties and has been the subject of much investigation. Using a small quantity, on a weight basis, of hydrogen as a supplement to gasoline was chosen as a way to extend lean engine operation. Onboard generation of hydrogen was selected as a feasible way to use hydrogen in a mobile application. The Jet Propulsion Laboratory conducted a similar program (refs. 6 and 7) in which hydrogen generated by the partial oxidation of gasoline was used as a fuel supplement for lean engine operation. Various

commercial processes to generate hydrogen were analyzed for their applicability. The catalytic steam reformation of methyl alcohol (methanol) using engine exhaust heat was selected as being the most efficient process to generate hydrogen that was also compact enough to be carried on a vehicle. One disadvantage is that it would require a second fuel and a second fuel system.

A research system to generate hydrogen by methanol reformation was built and installed on a multicylinder engine in an existing engine test setup. An independent and parallel program on catalyst evaluation was performed but is not part of this report. An engine test program was conducted using gasoline and additions of gaseous hydrogen and reformed methanol to evaluate the effects of hydrogen-gasoline fuel mixtures on exhaust emissions, extension of lean engine operating limits, and fuel flammability limits and combustion flame speed.

This report presents a brief description of the breadboard methanol reformation system and the results of fuel and engine testing.

The data were taken in the U. S. customary system of units and converted to SI units for this report.

EXPERIMENTAL APPROACH

Description of Engine

A 1969 high-compression-ratio (10. 5) Cadillac engine with a displacement volume of 7. 4 liters (472 in. ^{3}) was used as the test engine. All design characteristics of the engine are given in table I. Several interesting performance trade-offs are possible with a high-compression-ratio engine. The high peak combustion temperatures produce excessive oxides-of-nitrogen (NO_x) emissions at nominal equivalence ratios and, therefore, would seem to be inconsistent with reducing NO_x emissions. However, Bolt (ref. 8) noted that the lean-misfire limit could be significantly extended by increasing the compression ratio. The higher compression ratio produces higher temperatures at the start of combustion, which in turn causes higher flame speeds. Consequently, along with efficient operation at leaner equivalence ratios, high-compression-ratio engines might actually have lower NO_x emission levels than low-compression-ratio engines.

Single-cylinder, Comparative Fuels Research (CFR) tests performed by Lee (ref. 9) and Brehob (ref. 10) indicated that higher compression ratios at constant equivalence ratios slightly increased hydrocarbon emissions. Also, at ultralean conditions, the lower flame speeds raise exhaust manifold temperatures and produce excess oxygen, which may reduce hydrocarbon emissions. Hydrocarbon emission levels are also influenced by mixture uniformity and combustion chamber geometry. Both investigators found carbon monoxide emissions to be unaffected by compression ratio. The benefit of

high compression ratio on Otto-cycle efficiency is well recognized. This gain in efficiency might improve fuel economy at lean operation.

Fuels

The high-compression-ratio engine required a fuel with an octane rating of at least 96. The fuel used was a commercially available high-octane, lead-free gasoline; a chemical analysis of the fuel is provided in table II. The lower heating value was determined by the bomb calorimeter method, and the results were lower than expected. Each fuel batch was analyzed before use, and for some batches the lower heating value was determined by two laboratories. All results were within ±2.0 percent.

Of all the methods surveyed for the onboard generation of hydrogen, the steam reformation of methanol (CH_3OH; molecular weight, 32.042) appears to be the most efficient. It has the potential of exhaust energy recovery, and the 589 K (600° F) operating catalyst temperature is relatively low. The system converts waste thermal energy in the exhaust gases to useful chemical energy. A potential energy enrichment of 10 percent is possible.

A functional diagram describing the operation of the methanol reformer coupled to the engine and the breadboard components is shown in figure 1. The system was designed as a research apparatus and, therefore, no attempt was made to optimize size, weight, or catalyst material. In fact, other catalyst materials could result in more energy recovery and the use of smaller components. Performance instrumentation requirements also increased the physical size and weight of the system. A feedstock mixture consisting of 1.1 moles of water and 1.0 mole of methanol was selected. Bench tests had indicated that this ratio of methanol to water would produce the highest conversion efficiency and, therefore, the maximum volume flow of hydrogen to moles of mixture.

The mixture was pumped from the tank and evaporated in a counterflow heat exchanger heated by a small portion of the engine exhaust gases. The vaporizer heat exchanger consisted of 48 coils of 9.53-millimeter-diameter (0.375-in.-diam), helically wound tubing having a 6.99-centimeter (2.75-in.) mean diameter. A 0.51-millimeter-diameter (0.020-in.-diam) spring coil was inserted into the tube in order to promote swirl and to centrifuge the fluid to the tube walls. Hot gas was forced to pass over as much of the helical tube as possible. The tube was located midway in the annulus and permanently centered. It was separated from the 5.08-centimeter-diameter (2.0-in.-diam) center core and the 8.89-centimeter (3.5-in.) inner diameter of the outside shell by longitudinal 0.38-centimeter (0.15-in.) spacers.

The superheated mixture from the evaporator entered the catalyst chamber, which was heated by the same exhaust gas that had passed through the evaporator. Thirty-

seven 2.54-centimeter-diameter (1.0-in.-diam) tubes, with a length of 45.7 centimeters (18 in.), contained the tightly packed catalyst material. The catalyst material consisted of 3.2-millimeter-long (0.125-in.-long) pellets of manganese and copper. A catalyst material is usually selected for maximum hydrogen production at relatively low exhaust gas temperatures. Bench tests confirmed that 0.907 kilogram per hour of hydrogen (2 lb/hr) could be produced by the generator operating at 600° F (589 K). The catalyst chamber was 21.6 centimeters (8.5 in.) in diameter and 64.8 centimeters (25.5 in.) long and had a structural weight of 18.1 kilograms (40 lb). The unused engine exhaust gas bypassed the methanol reformer through a remotely adjustable valve. The bypass flow was combined with the gas used in the methanol reformer and then discharged to the atmosphere through the stock muffler and tailpipe.

An analysis of the possible reaction equations, described in the appendix, indicates that the catalyst, the mole reaction of methanol to water, and the percentage of the methanol-water feedstock that is converted to gaseous products can be selected to provide the desired engine operating conditions. For instance, these parameters would not be the same for maximum hydrogen production and maximum energy recovery from the exhaust gas. Also, some unconverted methanol could be used as an antiknock agent when using high compression ratios.

The reformed product gas, which consists of hydrogen, carbon monoxide, carbon dioxide, water, and methane, left the catalyst reformer at approximately 533 K (500° F). The specific composition of the product gas depended on the catalyst selected and the operating temperatures. The product gas was cooled to 389 K (240° F) by passing it through a heat exchanger located in the engine coolant flow system. This temperature was selected to avoid methanol and water condensation. Again, a design trade-off occurs. The temperature of the product gas entering the engine should be high enough to avoid water condensation. Also, higher initial mixture temperatures produce higher flame speeds. However, the higher mixture temperature increases the knocking tendency and reduces volumetric efficiency. The cooled, reformed product gas was then introduced into the engine in a plenum between the fuel atomizer and the inlet manifold. Product-gas flow rates were controlled by the feedstock flow rate, and the reformer system pressure was controlled by a variable-pressure regulator located in the reformed-product-gas line. Figure 2 shows the components of the methanol reformer system in relation to the Cadillac engine.

The engine was operated with varying amounts of bottled hydrogen added to gasoline in order to provide a basis for performance comparisons with the reformer experiments. A hydrogen supply line was connected to the plenum at the same location used by the reformer. The supply line contained a flowmeter and a flow-rate control valve. The bottled hydrogen was introduced into the intake manifold at ambient temperatures that were considerably lower than the 389 K (240° F) reformer-product-gas inlet temperature.

Test Procedure

The dynamometer load, or torque, and the engine speed were set to simulate an actual vehicle speed of 88.5 kilometers per hour (55 mph). All accessories were considered to be in operation and consuming engine power. Vehicle specifications required a brake horsepower of 26.9 kilowatts (36 bhp). The engine torque and engine speed were maintained constant at 119.3 joules (88 ft-lb) and 2140 rpm, respectively, for all equivalence ratios by an automatic engine throttle control system. This had the effect of simulating a constant vehicle speed for all equivalence ratios. The fuel-air mixture ratio was automatically adjusted and established by a commercially available atomizer and control system. Fuel at low pressure was atomized and entered a swirl chamber, where further evaporation and mixing occurred. The controller set and maintained a mixture ratio by continuously measuring the air and gasoline flow rates. This system replaced the stock carburetor as an efficient means to vary mixture ratio. Finally, the atomizer was installed on the stock intake manifold.

The lean operating limit was defined as the equivalence ratio where engine torque and engine speed could not be maintained by further opening of the throttle. This lean-limit equivalence ratio was considerably leaner than the equivalence ratio corresponding to the minimum drivability limit. A real-time IMEP instrument developed at the Lewis Research Center was used to identify misfire conditions.

The ignition timing was adjusted for minimum energy consumption at constant equivalence ratios. This was done by removing the vacuum advance tube from the distributor and rotating the distributor with a remotely controlled actuator. Therefore, the term "minimum energy consumption" as used in this report refers to the minimum energy consumption at some equivalence ratio where each energy consumption value has been minimized with respect to spark timing. Also, the equivalence ratio is defined as the wet fuel-air ratio divided by the stoichiometric fuel-air ratio of the fuel or combination of fuels used.

Apparent Flame Speed

The experimental approach used to evaluate the benefits and limitations of hydrogen-gasoline mixtures was to relate the emissions levels and the energy consumption to parameters defining the combustion process and the loss components. Combustion flame speed was selected as one way of relating relative combustion and engine performance. Apparent flame speed as used in this report is defined as the average velocity of the flame as it travels from the spark plug to the innermost piston/cylinder location. The combustion interval is the measurement of time used to determine the apparent flame speed. It is based on the mass of fuel burned (in percent) calculated from oscilloscope

traces of combustion chamber pressure versus crank angle. The procedure for determining the apparent flame speed was as follows: Combustion chamber pressure was measured by a piezoelectric quartz pressure transducer installed in a small chamber connected to the spark plug. The frequency response of the pressure measurement, including tube and sensor, was 2000 hertz and was computed on a calibration stand that produced a known pneumatic square wave. Also, the complete pressure-sensing system was checked for phase errors between the pressure signal and the crank-angle signal by the methods defined by Lancaster, Krieger, and Lienesch (ref. 11). Continuous phase shift and time response checks were performed on the running engine by shorting the spark plug and thereby checking for zero area on a pressure-volume display. The pressure signal was displayed on the Y-axis of pressure-versus-crank-angle and pressure-versus-volume oscilloscope traces. A three-output function generator was connected to the engine shaft. The signals produced were a linear voltage with crank angle, which was used as the oscilloscope X-axis sweep signal; 10-degree-interval, crank-angle markers; and the piston-swept volume signal. The display, as in figure 3, of chamber pressure versus crank angle, for several successive engine cycles, was photographed for analysis of the percentage of the mass burned.

The methods in the literature (refs. 12 to 17) for computing the percentage of the mass burned were surveyed. Each method had advantages and disadvantages, usually depending on the difficulty of obtaining thermodynamic property data and the complexity of the calculations. For this work, the method of Rassweiler and Withrow (ref. 12) appeared to offer an accurate and efficient method of analyzing the pressure-versus-crank-angle oscilloscope traces. The Rassweiler-Withrow method computes a difference in pressure - the pressure component due to combustion minus the pressure component due to piston motion for unburned conditions. The piston-motion pressure component is calculated by using adiabatic conditions over a small crank-angle interval. The pressure at the end point of this interval depends on the initial and final volume ratio raised to a power equal to the specific heat ratio. The pressure difference is multiplied by a factor that depends on the magnitude of the volume at the time of ignition in order to calculate constant-volume combustion at each crank-angle interval. Each pressure difference is added to the preceding value to result in a continuous summing process as a function of crank-angle rotation. Finally, the sum reaches a maximum value which, in turn, defines the completion of combustion or the crank angle where 100 percent of the mass of the charge is burned. The percentage of the mass burned at any point in the combustion interval is the sum of the pressure differences, at that crank angle, divided by the maximum summation value.

The percentages of the mass burned were computed from oscilloscope traces of combustion chamber pressure versus crank angle (fig. 3). These traces were read by moving a digital cursor over the pressure trace. The reading obtained by the cursor was used as input data to a computer that was programmed with the Rassweiler-Withrow

method. The output consisted of a graph and a table of the percentage of the mass burned, the percentage of the volume burned, and the derivative of pressure with respect to crank angle $dP/d\theta$ for crank-angle intervals of approximately 1 degree. Figure 4 is a typical graph of the output for gasoline-air combustion at an equivalence ratio of 0.82.

The combustion interval, in crank-angle degrees, was also calculated by the computer and was defined as the crankshaft rotation that occurred during combustion of 10 to 90 percent of the mass. The crank angle at 90 percent of the mass burned was also used to determine the maximum length of a line originating at the spark plug and ending at a point on the circumference of the piston. This distance was used as the maximum distance the flame traveled during normal combustion and was found to be about 10.2 centimeters (4 in.) or about equal to the bore for a wedge-shaped head. Changes in the equivalence ratio from rich to lean conditions produce sizable changes in the combustion interval. However, for these combustion intervals, the vertical motion of the piston with changes in crank angle is relatively small. Hence, the flame travel distance varies slightly with equivalence ratio. Based on the preceding assumptions, the apparent flame speed could be defined according to the relation

$$U_f = \frac{6N_E X}{\Delta\theta_c}$$

where

U_f apparent turbulent flame speed, m/sec (ft/sec)

N_E engine speed, rpm

X maximum distance traveled by flame, cm (in.)

$\Delta\theta_c$ combustion interval, deg

The apparent flame speed was calculated at each equivalence ratio and for each fuel. It was used to describe the variations in energy consumption and emissions levels between the different fuels.

Indicated Thermal Efficiency and Energy Balance Measurements

Two separate calculations were made of indicated mean effective pressure (IMEP). Oscilloscope traces of pressure versus crank angle and pressure versus volume were photographed simultaneously. Therefore, cycle-to-cycle variations in IMEP determined from the pressure-versus-volume traces could be correlated with cycle-to-cycle

variations in apparent flame speed. Again the analysis of the accuracy of the complete pressure-measuring system was performed in the manner reported in reference 11. The results indicated that no phase errors existed between the pressure, volume, and crank measurements. A second IMEP calculation was made with an instrument presently under development at the Lewis Research Center. This instrument records, in real time, 100 successive pressure-versus-volume traces. The IMEP was calculated for each cycle, and then an average value and a standard deviation were determined for all 100 cycles. The instrument output was displayed on an analog meter and indicated average IMEP in psi. A bar graph of all 100 IMEP calculations was displayed on a second oscilloscope. The bar graph is very useful in determining misfire conditions and cycles that have very poor combustion. A negative IMEP corresponds to the pumping IMEP and signifies a misfire condition. Figure 5 shows how the IMEP bar graphs vary with equivalence ratio when the engine is operating on gasoline. Figure 5(f) is an IMEP bar graph recorded near the lean limit and showing a misfire cycle.

An energy balance was performed to determine how the various loss components vary with equivalence ratio. At the same equivalence ratio, the apparent flame speed and the lean flammability limit are different for each fuel. Also, because the stoichiometric fuel-air ratio differs with each fuel, the magnitudes of the air and fuel flows at similar equivalence ratios will vary for the different fuels. Hence, a knowledge of how the loss components vary between the fuels would help in understanding the relation of total energy consumption to equivalence ratio. The energy balance used is a simple measurement of the energy in minus the energy out. The measured components that make up part of the energy balance are the input horsepower and the indicated horsepower. Also, a flowmeter and coolant thermocouples were installed in the cooling system to measure the energy absorbed by the coolant. However, radiation losses and energy absorbed by the lubrication system were not measured. The energy balance was checked in the following manner, which also showed the effect of not measuring these loss components: When the input energy, the power absorbed, and the energy lost to the coolant system are known, the energy remaining in the exhaust gases can be calculated. This energy is compared with a value computed from the exhaust flow rate, the average exhaust temperature at the exhaust valve, and the exhaust specific heat calculated from the Lewis chemical equilibrium program (ref. 18). The energy balance check showed an unbalance of 10 to 15 percent at both rich and lean conditions. However, it can still be used to indicate the trends of the various losses.

Emission Measurements

A Scott exhaust gas analysis system, Model 108-H, was used to measure emission levels. This system consists of nondispersive infrared measurements for carbon

monoxide and carbon dioxide emissions. Flame ionization methods were used to determine hydrocarbon emissions; the concentrations were measured in parts per million of equivalent propane gas. The nitric oxide (NO) emissions were measured with chemiluminescent techniques, and the oxygen concentration was measured by using paramagnetic effects. Known concentrations of gases were used to check the accuracy and calibrate the various constituents of the emissions measurement system. Several operational techniques were established to ensure good accuracy and trouble-free operation. First the sample line was heated to 450 K (350° F). Also, the internal sample lines used to measure the hydrocarbon and NO_x emissions were heated to 433 K (320° F). As part of the effort to avoid hydrocarbon and nitrogen dioxide (NO_2) dropout due to moisture removal, these emissions levels were determined on a wet basis. All other emissions levels were determined on a dry basis. Calibrations using the known gases were made just before taking a data point. Nitrogen gas was used to zero the instrumentation and to provide a continuously flowing purge through all systems except when a sample was taken. This technique eliminated contamination in the system. Finally, the converter used to convert NO_2 to NO was made of molybdenum in order to achieve high conversion efficiencies, as noted in reference 19. A stainless-steel converter had given erroneously low emissions readings because of its very low efficiency in converting NO_2 to NO. The system precision for all emission components was ±5 percent.

The hydrocarbon, carbon monoxide, carbon dioxide, and oxygen concentrations were used to determine the experimental fuel-air ratio based on the Spindt method (ref. 20). This calculation provides a check on the measured fuel and air mass flow rates. The measured fuel-air ratios and the values calculated by the Spindt method differed by 4 to 5 percent, with the Spindt value being consistently high at both rich and lean conditions.

RESULTS AND DISCUSSION

Energy Consumption

Flame speed. - Theoretical cycle analyses show that, for similar compression ratios and heat additions, constant-volume combustion processes are the most efficient. The reasons are that the maximum possible expansion of the working fluid occurs at high temperatures and that a minimum amount of heat is rejected. Consequently, high-flame-speed combustion processes, which closely approximate constant-volume processes, should result in high efficiencies. The effect of flame speed on efficiency is important in lean-mixture-ratio combustion because the flame speed decreases as the equivalence ratio decreases. In fact, the condition of zero flame speed is the theoretical

lean flammability limit.

The effect of adding hydrogen to gasoline on apparent turbulent flame speed is shown in figure 6. The hydrogen flow rate was set at a constant value of 0.64 kilogram per hour (1.42 lb/hr) for all equivalence ratios. For the gasoline and hydrogen-gasoline test points, the ignition timing was adjusted at each equivalence ratio for minimum fuel consumption. These different flow conditions define the mass fraction of hydrogen consumed f as the bottled-hydrogen flow rate divided by the sum of the hydrogen-gasoline flow rates. The values of f varied slightly with equivalence ratio, with the highest value of 0.068 occurring at the leanest equivalence ratios and the lowest value of 0.063 at the richest ratios. The brake horsepower was maintained at a constant value of 26.9 kilowatts (36 bhp) for all test points.

Adding hydrogen to gasoline significantly increased the apparent flame speed. This increase occurred at all equivalence ratios but was especially noticeable at lean equivalence ratios. At an equivalence ratio of 0.66, which is close to the lean-limit equivalence ratio of gasoline, the apparent flame speed was 61 percent faster with hydrogen enrichment. To verify the magnitude of the increase in flame speed for hydrogen-gasoline over that for gasoline, a search was made of engine flame speed data in the literature. This review showed that two types of turbulent flame speed relation exist. The first type states that the ratio of turbulent-to-laminar flame speed varies only as the engine speed or as the turbulence due solely to piston motion. The second type of relation states that the turbulent flame speed has a component due to the laminar flame speed and a component due to the engine Reynolds number. The engine Reynolds number, in turn, depends on the mean piston speed, the diameter of the inlet valve, the kinematic viscosity of inlet charge, and the inlet valve lift. Consequently, both types of relation state that the variations in turbulent flame speed with equivalence ratio and fuel composition are described by the variations in laminar flame speed with equivalence ratio and fuel composition. Variations in turbulent flame speed with chamber turbulence depend on the engine speed, the inlet valve characteristics, and the kinematic viscosity of the inlet charge. The tests described in this report were made at constant engine speed and constant inlet valve characteristics, and the differences in the viscosities of the fuels were considered to be small. Therefore, the differences in apparent flame speed between hydrogen-gasoline and gasoline should be explained by the differences in laminar flame speed with equivalence ratio for the two types of fuel.

The variation in laminar flame speed with equivalence ratio for hydrogen-gasoline and gasoline is shown in figure 7. The laminar flame speed theory of Semenov, Zeldovich, and Frank-Kamenetsky was used to determine the laminar flame speeds, as described by Barnett and Hibbard in reference 21. The results show that the laminar flame speed is greater for hydrogen-gasoline than for gasoline. However, the difference is almost insignificant at equivalence ratios below 0.75. This disagrees with the results of figure 6, where the greatest differences in apparent flame speed between hydrogen-

gasoline and gasoline occur at equivalence ratios below 0.75. Also, the maximum difference in laminar flame speed (fig. 7) is about 8 percent, at an equivalence ratio of about 1.05. At the same equivalence ratio the difference in apparent turbulent flame speed (fig. 6) is approximately 19 percent. It becomes apparent that variations in turbulent flame speed with equivalence ratio cannot be singularly described by variations in laminar flame speed with equivalence ratio. Complicating factors are, for example, the turbulence generated by the advancing flame front and the very large turbulence scale or swirl effects. These factors will not allow a simple description of the turbulent flame speed, such as, that the turbulent flame speed is proportional to the sum of the laminar flame speed plus a simple perturbation factor. It is also important to consider the validity of the Semenov theory to describe the laminar flame speed with equivalence ratio. Many investigators have shown agreement between this theory and experiment. However, the Semenov theory, while accounting for molecular diffusion, neglects the diffusion of free radicals, which is known to affect the developing flame speed. Finally, comparing figures 6 and 7 shows that, for both turbulent and laminar flames, hydrogen-gasoline has a higher flame speed than gasoline.

The effect of adding hydrogen on gasoline's apparent flame speed is contained in the factors that control the rate of the combustion process. The flame velocity depends on the rate of thermal and mass transport from the burned to the unburned gas. This, in turn, depends on the heat and mass transfer across the flame front. At the same equivalence ratio, hydrogen induces higher flame temperatures, which increases the difference between the temperatures of the burned and unburned mixtures and creates a more efficient heat-transfer mechanism. This same temperature difference explains some of the reduction in flame speed with leaner equivalence ratios. As the charge gets leaner, the flame temperature decreases, which, in turn, lowers the heat transfer to the unburned mixture. Other important factors that control heat transfer are the flame front area, the heat lost to the chamber walls, the gas emissivities, and the transport properties of the gaseous mixture. A second mode of energy transfer, mass transfer, is also affected by adding hydrogen. Molecular diffusion and the diffusion of active radicals due to concentration gradients between the burned and unburned mixtures, along with the physical transfer of burning particles into the unburned mixture, strongly influence flame speed. The chemical series of reactions involved in the combustion process is affected by the reaction kinetics, which depend on diffusion of these active radicals into the unburned mixture. Hydrogen possesses a high diffusion coefficient and may enter the chemical reaction systems in a manner that produces more active radicals. The transport of these radicals also depends on the motion of the gases either due to the motion of the flame front itself or due to externally induced small- and large-scale turbulence.

Ignition delay. - The ignition delay period is defined as the time from ignition until 10 percent of the mass is burned. It is a function of the chemical reactions in the com-

bustion chamber and, in particular, near the ignition source. The exact mechanism of ignition delay is still unknown. However, the author and others believe that some intermediate products of combustion are generated in this period that may be required to achieve a self-sustaining reaction. A simpler description of ignition delay involves the stagnant boundary layer near the spark plug and the chamber wall. The ignition delay period is characterized by slow combustion within the volume containing the spark plug and the quiescent wall boundary layer. The energy release is extremely restricted within this volume for a period of time. Variations in the ignition delay period may cause cycle-to-cycle variations in peak cylinder pressure and IMEP. Figure 8 shows a sizable reduction in ignition delay time with the addition of hydrogen for all equivalence ratios. The advantageous thermal properties of hydrogen appear to diminish the thermal loss from the developing flame kernel and to quicken the energy release rate.

Flame speed and energy balance. - The distribution of engine energy among the various losses associated with engine operation was correlated with the calculated apparent flame speed for gasoline and hydrogen-gasoline. The combustion temperature must be known to explain flame speed and the differences in losses between the two fuels. Since the combustion temperature was not measured, theoretical adiabatic flame temperatures were calculated for the range of equivalence ratios tested by using the Lewis chemical equilibrium program (ref. 18). These temperatures are shown in figure 9 as a function of apparent flame speed calculated from the test points for gasoline and hydrogen-gasoline. These flame temperatures are theoretical, but combustion temperatures in real engines would probably show similar trends with both gasoline and hydrogen-gasoline. For the same apparent flame speed, which occurs at markedly different equivalence ratios, gasoline has a higher combustion temperature. However, for the same equivalence ratio, the theoretical adiabatic flame temperature is slightly lower for gasoline than for hydrogen-gasoline.

Table III shows the various components used in the energy balance. The components with and without hydrogen enrichment are compared at three equivalence ratios. The 0.80 and 0.69 equivalence ratios were chosen because they are the minimum-energy-consumption ratios for gasoline and hydrogen-gasoline, respectively. The 0.98 equivalence ratio was chosen because at this ratio the apparent flame speed for gasoline is the same as that for hydrogen-gasoline as its minimum-energy-consumption equivalence ratio of 0.69. Therefore, the second and last rows represent the special case of identical flame speeds for hydrogen-gasoline and gasoline. As previously noted and shown in figure 6, adding hydrogen significantly increases apparent flame speed. This same effect is noted in table III, where at each equivalence ratio adding hydrogen produces a higher flame speed. The higher flame speeds resulting from adding hydrogen produce larger energy losses to the cooling system. Higher flame speeds correspond to higher combustion temperatures, which, in turn, force larger energy losses to the cooling system.

At the same equivalence ratio, the energy lost to the exhaust flow is less with hydrogen-gasoline than with gasoline. However, both fuels have about the same energy loss to the exhaust flow at equivalence ratios above 0.80. At this equivalence ratio, both fuels have high apparent flame speeds, which, in turn, cause less energy to be lost to the exhaust flow. At the 0.69 equivalence ratio, the flame speed with hydrogen-gasoline is 61 percent higher than with gasoline. At this equivalence ratio, the energy lost to the exhaust flow with hydrogen-gasoline is 37 percent less than with gasoline.

The required input energy is the sum of all the loss components. At equivalence ratios below 0.80, hydrogen-gasoline requires less input energy because the much higher flame speeds cause less energy to be lost to the exhaust flow. At equivalence ratios above 0.80, there is a slight increase in the input energy required for hydrogen-gasoline. This increase is again due to the higher flame speeds of hydrogen-gasoline producing higher combustion temperatures and larger losses to the cooling system.

Another interesting comparison to make in table III is between the flame speeds in the second and the last rows. A flame speed of approximately 34 meters per second (113 ft/sec) occurs at an equivalence ratio of 0.69 for hydrogen-gasoline, but at an equivalence ratio of 0.96 for gasoline. For this case, less energy loss to the cooling system occurs with hydrogen-gasoline. This then poses the question, "Can two fuels exhibiting the same apparent flame speed produce different combustion temperatures?" Apparent flame speed as a function of equivalence ratio calculated in the Lewis chemical equilibrium program (ref. 18) was combined with the results of figure 6 to form figure 9. It shows the variation of adiabatic flame temperature with flame speed for the two fuels. At the same flame speed, gasoline has the higher adiabatic flame temperature. This is consistent with the higher energy losses to the cooling system with gasoline, as noted in table III for the constant-flame-speed comparisons. This same effect is reflected in the higher exhaust manifold temperature for gasoline (last column of table III).

Total energy consumption. - The total energy consumption was obtained over a range of equivalence ratios for gasoline, gasoline with bottled hydrogen, and gasoline with hydrogen produced by the methanol reformer. A sample analysis of the reformed methanol product gas is contained in table IV, which shows the composition, the mole fraction, the flow rate, and the energy content. For a conversion efficiency of 37 percent, a hydrogen flow rate of 0.231 kilogram per hour (0.51 lb/hr) was produced, and the gain in energy due to the system's endothermal reactions was approximately 3 percent. The total energy consumption was computed by multiplying the gasoline flow rate by its lower heating value and adding the product of the liquid-methanol flow rate into the reformer and its lower heating value of 4802 joules per gram (8644 Btu/lb).

The energy consumption plotted as a function of equivalence ratio in figure 10 shows that the minimum energy consumption is the same for each fuel. However, the minimum energy consumption occurs at lower equivalence ratios for both hydrogen-gasoline

mixtures than for gasoline. The minimum-energy-consumption equivalence ratio is lowest for gasoline with bottled hydrogen because the hydrogen flow rate of 0.635 kilogram per hour (1.4 lb/hr) is faster than the 0.231 kilogram per hour (0.51 lb/hr) produced by the methanol reformer. As previously discussed, adding hydrogen causes higher apparent flame speeds, which, in turn, control the amount of input energy lost to the exhaust gas and to the cooling system. The higher apparent flame speed occurring with the 0.635-kilogram-per-hour (1.4-lb/hr) hydrogen flow (table III) accounts for the slight increase in total energy consumption for gasoline with bottled hydrogen at equivalence ratios from 0.74 to 1.05. This increase in energy consumption occurs as an increase in energy loss to the cooling system. Total energy consumption is significantly lower at equivalence ratios below 0.70 for both hydrogen-gasoline mixtures at the same flow rate. It appears that modest additions of hydrogen increase the flame speed sufficiently to allow smooth and efficient lean operation.

The energy consumption data presented in figure 10 were obtained on different days. For gasoline and gasoline with bottled hydrogen, the tests were repeated to give confidence in the results. Before operating the engine with either hydrogen-gasoline mixture, energy consumption, emissions, and performance data were obtained with gasoline to ensure that the gasoline data did not vary. The curves of figure 10 represent a least-squares fit to the experimental data.

As mentioned previously the ignition timing was adjusted to minimum energy consumption at a fixed equivalence ratio. However, the coupling of the methanol reformer to the engine through the exhaust flow and the inlet manifold flow made ignition timing changes very difficult for the gasoline-with-reformed-hydrogen cases. Consequently, the timing used for those cases was that used for gasoline. The ignition timing angles were 48° advance for gasoline and gasoline with reformed hydrogen. The timing angles for gasoline with bottled hydrogen varied from 23° advance at rich equivalence ratios to 54° at the lean limit.

Indicated thermal efficiency. - The improvement in indicated thermal efficiency with the addition of hydrogen to gasoline is shown in figure 11. Adding either bottled hydrogen or hydrogen from reformed methanol allows leaner equivalence ratios from reduced loss to the exhaust gas as the flame speed increases. Again, the lower hydrogen flow rates produced by the reformer still provide efficient operation at this constant energy level. At equivalence ratios greater than 0.85, all the fuels increased the flame speed (higher combustion temperature), which caused more energy to be absorbed by the cooling system. This condition causes, in turn, a general decrease in thermal efficiency with increasing equivalence ratio.

Emission Results

Oxides-of-nitrogen emissions. - The emission levels of NO_x as a function of equiv-

alence ratio for gasoline and hydrogen-gasoline are given in figure 12. Extending the efficient operating range into leaner mixtures by mixing hydrogen with gasoline reduces NO_x emission levels considerably. A reduction by a factor of 2 in NO_x levels is shown in figure 12 when comparison is made on the basis of minimum-energy-consumption equivalence ratios. The stock, 1969 high-compression-ratio engine, which does not have NO_x emission controls, operates at an equivalence ratio of 0.94 at the simulated road-load condition. Comparing NO_x levels at the 0.94 equivalence ratio and the minimum-energy-consumption equivalence ratio of 0.66 for hydrogen-gasoline shows an even larger reduction, by a factor of 5. Even more dramatic reductions in NO_x levels occur if the hydrogen-gasoline equivalence ratio is extended to equivalence ratios below 0.60. Operating at equivalence ratios between 0.55 and 0.60 reduces NO_x emissions by a factor of 19, but with an increase of 3 to 6 percent in energy consumption over the minimum. However, the problems of reduced vehicle drivability at lean equivalence ratios limits the extent of lean operation and, therefore, the possible NO_x emission reduction. Smooth engine operation, defined as operation without any engine vibrations or power surging and with good power response, deteriorated rapidly at equivalence ratios below the minimum-energy-consumption values. The explanation is that lean operation reduces flame speeds and, therefore, decreases indicated power. This effect is magnified by variations in the fuel-air mixture ratio, which increase with leaner equivalence ratios and which occur on a cycle-to-cycle and cylinder-to-cylinder basis. Therefore, NO_x emission reduction comparisons should not be made at equivalence ratios below the minimum-energy-consumption values.

Figure 12 also indicates that, at similar equivalence ratios, hydrogen-gasoline produces higher NO_x levels than gasoline. This again can be explained by the higher peak combustion temperatures that occur with hydrogen-gasoline fuels as compared with gasoline operating at the same equivalence ratio.

The larger NO_x emissions produced by gasoline with reformed hydrogen are difficult to explain because the flame speed instrumentation was not available for these tests. The emissions analyzer was calibrated before each data point, and NO_x emission levels were measured with the engine running on gasoline before each reformer test in order to establish consistent emission levels between data runs. However, the reformer product gas entered the engine at a temperature of 389 K (240° F), which raised the total inlet temperature. This higher inlet temperature would increase the peak combustion temperatures and thus explain the higher NO_x emission levels.

Hydrocarbon emissions. - The hydrocarbon emission levels are plotted as a function of equivalence ratio in figure 13. The hydrocarbon emission levels are characterized as parts per million of equivalent propane (C_3H_8), and the flame ionization detector was calibrated with gases containing known concentrations of ppm C_3H_8 in air. Figure 13 shows that the hydrocarbon emission levels of hydrogen-gasoline are slightly higher than gasoline levels when the comparison is made at the minimum-energy-consumption equiv-

alence ratios. However, the increase in hydrocarbon emissions is not as large as generally reported by investigators using lower-compression-ratio engines. Again, the deteriorating vehicle drivability below the minimum-energy-consumption equivalence ratios makes hydrocarbon emission level comparisons below these equivalence ratios meaningless. Comparisons based on the same equivalence ratio show that, at ratios above 0.80, hydrogen-gasoline produced lower hydrocarbon emission levels. Again, this condition is different from results reported by investigators using lower-compression-ratio engines, where the hydrogen-gasoline hydrocarbon levels are higher than gasoline levels at all equivalence ratios. Perhaps the higher combustion temperatures associated with higher compression ratios may alter the complex system of chemical reactions in such a way that less hydrocarbons are formed or that more hydrocarbons are oxidized into other components in the hydrogen-gasoline operation. A second possible explanation, confirmed by results from the chemical kinetics program of Bittker and Scullin (ref. 22) using methane-air and methane-hydrogen-air, is the formation of formaldehyde (CH_2O) with hydrogen enrichment. Formaldehyde can be considered as a hydrocarbon and would not be detected by flame ionization detector instrumentation. Thus, the rich equivalence ratio results of figure 13 for hydrogen-gasoline may be distorted by the inability to measure formaldehyde concentrations.

Carbon monoxide emissions. - The carbon monoxide emission levels as a function of equivalence ratio are shown in figure 14. Emission levels for gasoline with reformed hydrogen were similar to gasoline levels. As the equivalence ratio was extended to leaner values, the carbon monoxide levels remained fixed and low. Figure 14 also shows that gasoline with bottled hydrogen produced the lowest carbon monoxide emissions at all equivalence ratios. The formation of carbon monoxide is a complex process and is not understood for either gasoline or hydrogen-gasoline. Performing the same chemical kinetics study that was used to explain the hydrocarbon emissions (ref. 22) showed that the formation of formaldehyde and the HCO radical can lower the carbon monoxide concentration in hydrogen-gasoline.

Performance of methanol reformer. - The methanol reformer system was designed as a research tool to check and verify the concept of steam reformation of methanol as an efficient way to produce hydrogen. The size, weight, and location of components with respect to the engine were dictated by the desire to observe and measure the factors influencing the overall system performance. Certain control problems occurred. Instabilities originated either in the engine or the reformer system and were passed on to the other component, which changes a stable condition into an unstable one. For instance, if the engine surged because of misfire at lean operation, oscillations in the exhaust flow rate and the manifold pressure also occurred. Since the exhaust flow was used to heat the catalyst, these flow oscillations caused oscillations in the reformer-product flow rate. The reformer-product flow rate was partially controlled by the manifold pressure, so manifold instabilities augmented any existing reformer-product flow instabilities.

This type of reformer-engine system should contain an automatic closed-loop control; however, one was not available for this program.

A definite limitation of a methanol steam reformation system is the need for a second fuel and a second fuel system in the vehicle. With proper design and catalyst selection, this disadvantage may be offset by the prospect of recovering as much as 10 percent of the energy lost to the exhaust gas. Also, in view of decreasing petroleum resources, a system using 100-percent reformed methanol might be an interesting supplementary or alternative fuel system.

SUMMARY OF RESULTS

Apparent flame speed and energy balance measurements were used to explain performance and emissions differences between gasoline and gasoline enriched by bottled hydrogen and hydrogen produced by a methanol reformer.

For a single load and engine speed condition, a multicylinder engine operating with lean mixture ratios with and without hydrogen addition gave the following results:

1. Adding small amounts of hydrogen to gasoline produced efficient lean operation by increasing the apparent flame speed and reducing ignition lag.

2. The actual minimum energy consumption was the same for gasoline and hydrogen-gasoline, although the minimum-energy-consumption equivalence ratio decreased from 0.79 to 0.67.

3. Exhaust emissions levels followed the classical trends with changing equivalence ratio. Oxides-of-nitrogen emission levels at the minimum-energy-consumption equivalence ratios were appreciably lower for hydrogen-gasoline than for gasoline. At the same equivalence ratio, in the range of practical interest, NO_x emissions were higher for hydrogen-gasoline than for gasoline because of hydrogen's higher peak combustion temperatures.

4. Gasoline with reformed hydrogen gave the highest NO_x emission levels. The reformer must produce gas at a high enough temperature to avoid water or methanol condensation. The high inlet temperature can cause higher peak combustion temperatures and, therefore, higher NO_x emission levels.

5. The hydrocarbon emission levels of hydrogen-gasoline did not follow the trends reported from lower-compression-ratio engines, in that hydrocarbon emission levels were lower with hydrogen enrichment at equivalence ratios above 0.80. Hydrocarbon emission levels were somewhat higher for hydrogen-gasoline at minimum-energy-consumption equivalence ratios. However, the combustion process for gasoline with bottled hydrogen produced the lowest carbon monoxide emission levels.

6. The steam reformation of methanol is potentially an energy-conserving way to produce onboard hydrogen. A closed-loop control system is required to maintain engine

reformer stability and to optimize the total performance and efficiency of the combined reformer-engine system.

Lewis Research Center,
National Aeronautics and Space Administration,
Cleveland, Ohio, March 15, 1977,
505-05.

APPENDIX - HYDROGEN GENERATION BY STEAM REFORMATION OF METHANOL

The steam reformation of methanol uses the following chemical reaction system. A primary assumption is that the product gas, or constituents making up the right side of the equation, will consist of CH_3OH, H_2O, H_2, CO_2, CO, and CH_4. So

$$CH_3OH + (a)H_2O \xrightarrow{\text{Catalyst}} (b)H_2O + (c)CH_3OH + (d)H_2 + (e)CO + (f)CO_2 + (g)CH_4 \quad (1)$$

Equation (1) can also be considered in terms of a reactant solution consisting of M moles of CH_3OH plus W moles of H_2O. Then, if a dry analysis is made on the product gas, we define the following conversion factor:

$$Y_{\text{subscript}} = \text{Percentage of converted methanol per conversion reaction} \quad (2)$$

If this factor is determined experimentally, the conversion ratio X can be determined. On the basis of 1 mole of CH_3OH, equations (1) and (2), along with the conversion ratio X, form the following reaction:

$$CH_3OH + \left(\frac{W}{M}\right)H_2O \xrightarrow{\text{Catalyst}} \left\{\frac{W}{M} + X\left[Y_{CO_2}\left(\frac{W}{M} - 1\right) + Y_{CO}\frac{W}{M} + Y_{CH_4}\left(\frac{W}{M} + 1\right) - \frac{W}{M}\right]\right\}H_2O$$

$$+ (1 - X)CH_3OH + X\left(3Y_{CO_2} + 2Y_{CO} - Y_{CH_4}\right)H_2 + XY_{CO_2}CO_2$$

$$+ XY_{CO}CO + XY_{CH_4}CH_4 \quad (3)$$

Consequently, for a particular catalyst material and operating condition and the measured values of Y_{CO_2}, Y_{CO}, and Y_{CH_4}, the conversion ratio X is determined by

$$X = \frac{(\text{Total product moles per mole of } CH_3OH \text{ vapor}) - \left(\frac{W}{M} + 1\right)}{\left(\frac{W}{M} + 3\right)Y_{CO_2} + \left(\frac{W}{M} + 3\right)Y_{CO} + \left(\frac{W}{M} + 1\right)Y_{CH_4} - \left(\frac{W}{M} + 1\right)} \quad (4)$$

With X known, we can now determine the resulting individual constituent flow rates in the product gas.

It is also interesting to consider the difference in the lower heating values between the feedstock and the product gas. From equations (3) and (4) with the lower heating values of H_2, CO, and CH_4 and the bench tests that defined their concentrations in the

product gas, on a per-gallon-of-feedstock basis,

$$\begin{pmatrix}\text{Product-gas}\\ \text{lower heating}\\ \text{value}\end{pmatrix} = 278.7 \text{ J/liter} + 278.7(X) \text{ J/liter}$$

$$= 41\,686 \text{ Btu/gal} + 3499(X) \text{ Btu/gal} \qquad (5)$$

REFERENCES

1. Taylor, Charles F.: The Internal Combustion Engine in Theory and Practice. Vols. 1 and 2, 2nd ed., Mass. Inst. Tech. Press, 1968.

2. Yu, Henry T. C.: Fuel Distribution Studies - A New Look at an Old Problem. SAE Trans., vol. 71, 1963, pp. 596-613.

3. Hansel, J. G.: Lean Automotive Engine Operation - Hydrocarbon Exhaust Emissions and Combustion Characteristics. SAE Paper 710164, Jan. 1971.

4. Lewis, Bernard; and Von Elbe, Guenther: Combustion, Flames, and Explosions of Gases. Academic Press, 1961.

5. Stebar, R. F.; and Parks, F. B.: Emission Control with Lean Operation Using Hydrogen-Supplemented Fuel. SAE Paper 740187, 1974.

6. Hoehn, F. W.; and Dowdy, M. W.: Feasibility Demonstration of a Road Vehicle Fueled with Hydrogen-Enriched Gasoline. Ninth Intersociety Energy Conversion Engineering Conference. Am. Soc. Mech. Eng., 1974, pp. 956-964.

7. Hoehn, F. W.; Baisley, R. L.; and Dowdy, M. W.: Advantages in Ultralean Combustion Technology Using Hydrogen-Enriched Gasoline. Tenth Intersociety Energy Conversion Engineering Conference. Inst. Electr. Electron. Eng., 1975, pp. 1156-1164.

8. Bolt, J.; and Holkeboer, D.: Lean Fuel/Air Mixtures for High-Compression Spark-Ignited Engines. SAE Trans., vol. 70, 1962, pp. 195-202.

9. Lee, R. C.: Effect of Compression Ratio, Mixture Strength, Spark Timing, and Coolant Temperature upon Exhaust Emissions and Power. SAE Paper 710832, Oct. 1971.

10. Brehob, W.: Mechanisms of Pollutant Formation and Control from Automotive Sources. SAE Paper 710483, June 1971.

11. Lancaster, D. R.; Krieger, R. B.; and Lienesch, J. H.: Measurement of Analysis of Engine Pressure Data. SAE Paper 750026, Feb. 1975.

12. Rassweiler, G. M.; and Withrow, L.: Motion Pictures of Engine Flame Correlated with Pressure Cards. SAE Trans., vol. 42, no. 5, May 1938, pp. 185-204.

13. Krieger, R. E.; and Borman, G. L.: The Computation of Apparent Heat Release for Internal Combustion Engines. ASME Paper 66-WA/DGP-4, Dec. 1966.

14. Hiroyasu, Hiroyuki; and Kadota, Toshikazu: Computer Simulation for Combustion and Exhaust Emissions in Spark-Ignition Engine. Fifteenth International Symposium on Combustion. Combustion Inst. Press, 1974, pp. 234-236.

15. Samaga, B. S.; and Murthy, B. S.: On the Problem of Predicting Burning Rates in a Spark-Ignition Engine. SAE Paper 750688, June 1975.

16. McCuiston, F. D., Jr.: Validation of a Turbulent Flame Propagation Model for an Internal Combustion Engine. Ph. D. Thesis, Univ. Cincinnati, 1976.

17. Eyzat, P.; and Guibet, J. D.: A New Look at Nitrogen Oxides Formation in Internal Combustion Engines. SAE Paper 680124, Jan. 1968.

18. Gordon, Sanford; and McBride, Bonnie: Computer Program for Calculation of Complex Chemical Equilibrium Compositions, Rocket Performance, Incident and Reflected Shocks, and Chapman-Jouguet Detonations. NASA SP-273, 1971.

19. Summers, Robert L.: NO_x Destruction by CO in NO_x-to-NO Converters of Chemiluminescence NO Analyzers. NASA TM X-73480, 1976.

20. Spindt, R. S.: Air-Fuel Ratios from Exhaust Gas Analysis. SAE Paper 650507, May 1965.

21. Barnett, Henry C.; and Hibbard, Robert C., eds.: Basic Considerations in the Combustion of Hydrocarbon Fuels. NACA TR-1300, 1957.

22. Bittner, David; and Scullin, Vincent: General Chemical Kinetics Computer Program for Static and Flow Reactions, with Application to Combustion and Shock-Tube Kinetics. NASA TN D-6586, 1972.

TABLE I. - ENGINE SPECIFICATIONS

Bore, cm (in.)	10.92 (4.30)
Stroke, cm (in.)	10.31 (4.06)
Piston displacement, liter (in.^{3})	.74 (472)
Compression ratio	8.5
Horsepower at 4400 rpm, kW (bhp)	280 (375)
Torque at 3000 rpm, J (ft-lb)	712 (525)
Connecting rod length, cm (in.)	17.15 (6.75)
Inlet-valve diameter, cm (in.)	5.08 (2.00)
Exhaust-valve diameter, cm (in.)	4.13 (1.625)
Inlet-valve lift, cm (in.)	1.12 (0.440)
Exhaust-valve lift, cm (in.)	1.15 (0.454)
Valve rocket arm ratio	1.65
Valve timing:	
Intake valve opens, deg BTDC	18
Intake valve closes, deg ABDC	114
Exhaust valve closes, deg ATDC	58
Exhaust valve opens, deg BBDC	70

TABLE II. - CERTIFIED GASOLINE ANALYSIS

Specific gravity:	
At 283 K (50° F)	0.788
At 289 K (60° F)	0.784
At 294 K (70° F)	0.780
At 300 K (80° F)	0.775
Distillation (ASTM D86):	
Indicated boiling point, K (°F)	773 (932)
10-Percent evaporation, K (°F)	335.3 (143.6)
30-Percent evaporation, K (°F)	367.3 (201.2)
50-Percent evaporation, K (°F)	385.3 (233.6)
70-Percent evaporation, K (°F)	448.3 (347.0)
90-Percent evaporation, K (°F)	459.3 (366.8)
Evaporation point, K (°F)	
Amount recovered, percent	96
Residue, percent	1.5
Amount lost, percent	2.5
Reid vapor pressure (ASTM D323), Pa (psi)	44 127 (6.4)
Research octane number	101.3
Motor octane number	90.1
Lead content, g/100 cm^3	0.0001
Sulfur content, mg/cm^3	<0.04
Gum content, mg/100 cm^3:	
Before washing	7.2
After washing	<1
Lower heat of combustion, J/kg (Btu/lb)	41 425 496 (17 811)
Aromatics content, vol %	50.1
Olefins content, vol %	2.1
Paraffin content, vol %	47.8
Carbon content, wt %	88.86
Hydrogen content, wt %	11.80

TABLE III. - ENGINE ENERGY BALANCE

Hydrogen addition[a]	Equivalence ratio	Apparent flame speed		Input energy		Energy lost to cooling system		Energy lost to exhaust		Indicated horsepower		Brake horsepower		Exhaust manifold temperature	
		m/sec	ft/sec	kW	hp	kW	hp	kW	hp	kW	hp	kW	hp	K	°F
No	0.69	22	71	131	175	39	52	51	68	35	47	27	36	989	1322
Yes	[b]0.69	35	114	118	158	42	56	32	43	37	50	27	36	896	1153
No	[b]0.80	31	100	118	158	41	55	37	49	34	46	27	36	969	1286
Yes	0.80	40	132	122	163	45	60	33	44	37	50	27	36	943	1238
Yes	0.98	45	146	126	169	49	65	35	47	37	49	27	36	986	1315
No	0.96	34	113	122	164	46	62	34	46	37	49	27	36	981	1306

[a]Flow rate, 0.635 kg/hr (1.4 lb/hr).

[b]Minimum-energy-consumption equivalence ratio.

TABLE IV. - REFORMER ANALYSIS

[Conversion efficiency, 37 percent.]

Component	Content		Flow rate		Energy	
	mole per mole of methanol	mole fraction	kg/hr	lb/hr	J/min	Btu/min
Reactant						
Methanol	1.0	----	3.77	8.34	1 259 670	1194
Water	1.1	----	2.33	5.16	---------	----
Product gas						
Methanol	0.63	----	2.37	5.22	858 770	814
Water	.87	----	1.83	4.02	---------	----
Hydrogen	.97	70.4	.23	.51	461 035	437
Carbon monoxide	.14	11.0	.46	1.02	75 960	72
Carbon dioxide	.23	18.6	1.21	2.64	---------	----
Methane	0	0	0	0	---------	----
Total	----	----	----	----	1 395 765	1323

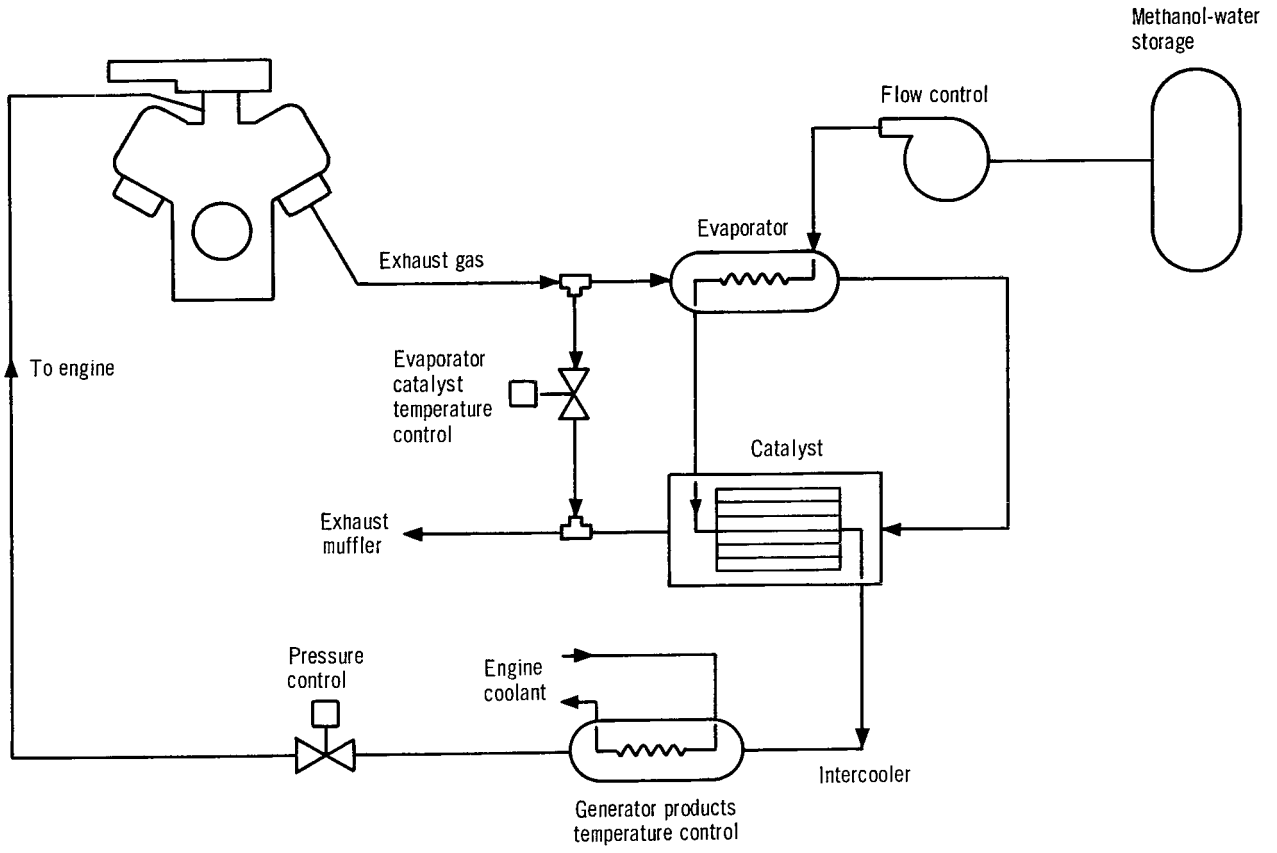

Figure 1. - Schematic diagram of methanol reformer system.

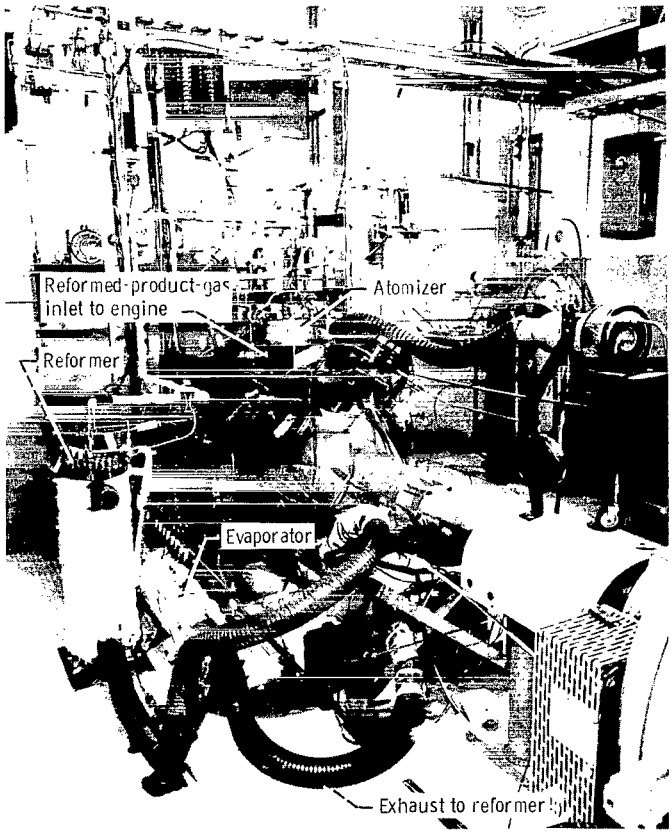

Figure 2. - Methanol reformer system in relation to engine.

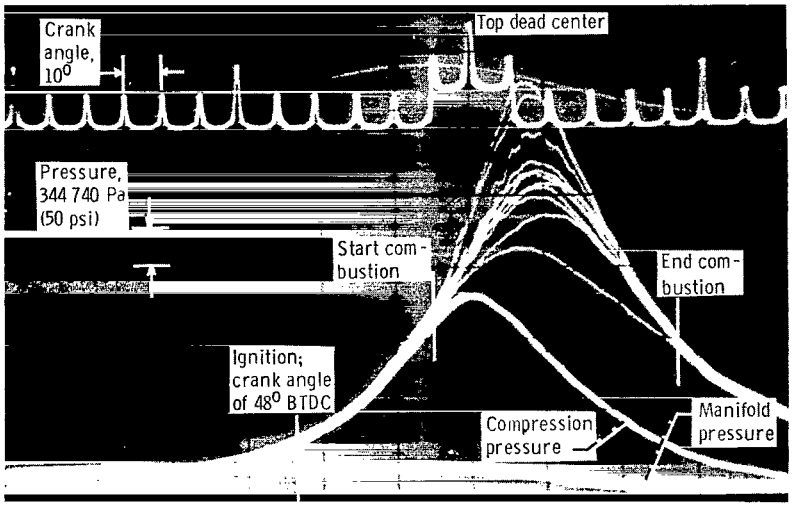

Figure 3. - Oscilloscope traces of chamber pressure as function of crank angle. Engine, 1969 Cadillac; brake horsepower, 27 kW (36 bhp); engine speed, 2140 rpm; fuel, gasoline; equivalence ratio, 0.87.

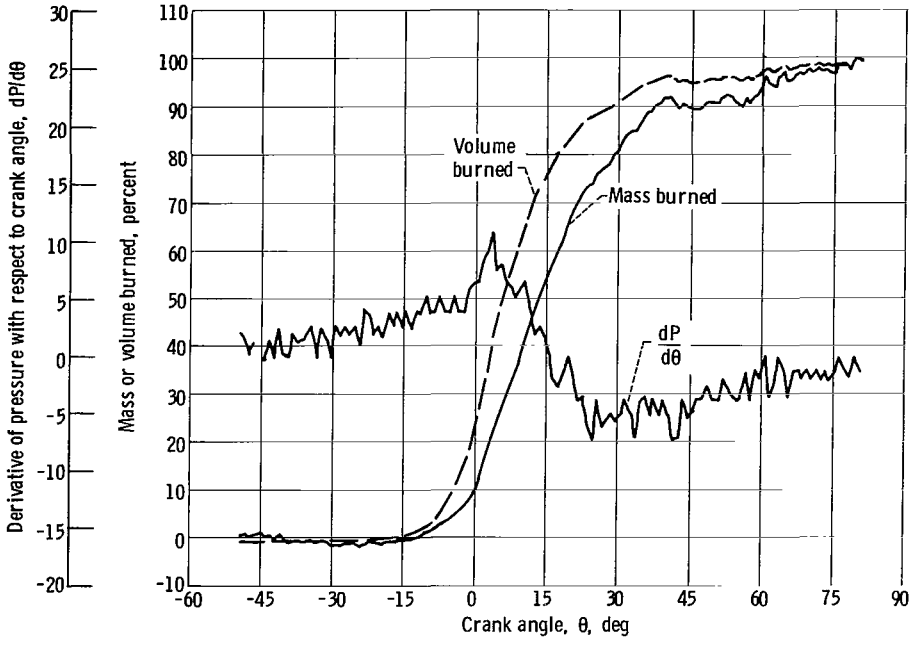

Figure 4. - Computer output showing percentages of mass and volume burned and derivative of pressure with respect to crank angle for gasoline-air combustion at equivalence ratio of 0.82.

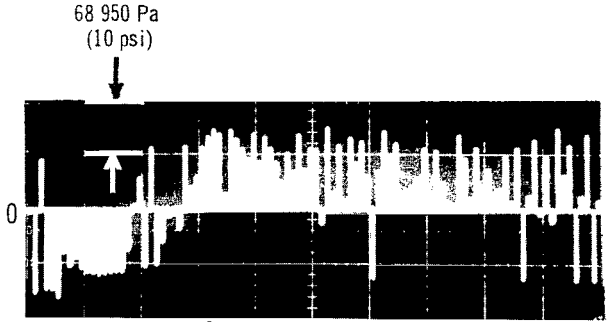

(a) Engine startup. Mean, 22 063 Pa (3.2 psi); standard deviation, 64 811 Pa (9.4 psi).

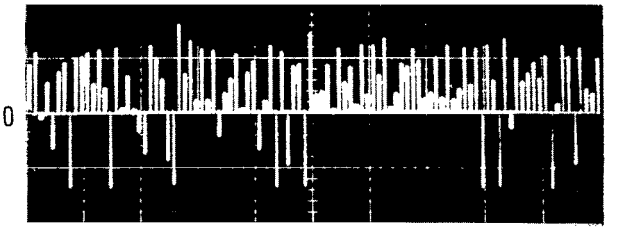

(b) Idle. Engine speed, 1000 rpm; mean, 31 716 Pa (4.6 psi); standard deviation, 53 779 Pa (7.8 psi).

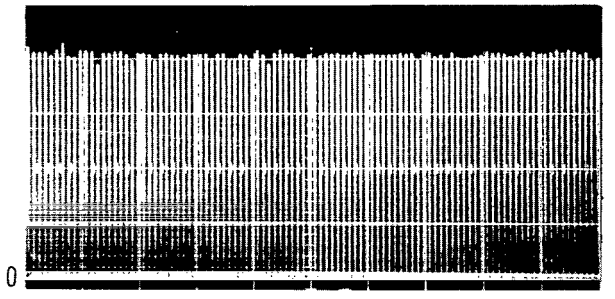

(c) Engine speed, 2140 rpm; torque, 119 J (88 ft-lb); equivalence ratio, 1.0; mean, 282 687 Pa (41.0 psi); standard deviation, 4826 Pa (0.7 psi).

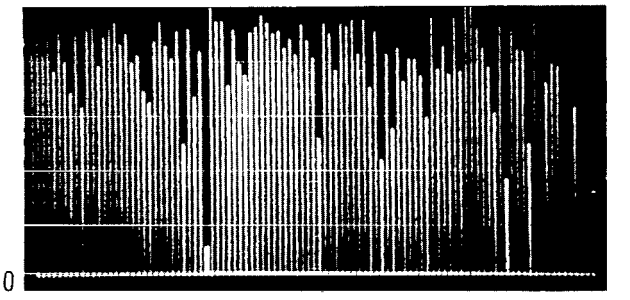

(d) Engine speed, 2140 rpm; torque, 119 J (88 ft-lb); equivalence ratio, 0.81; mean, 286 134 Pa (41.5 psi); standard deviation, 52 401 Pa (7.6 psi).

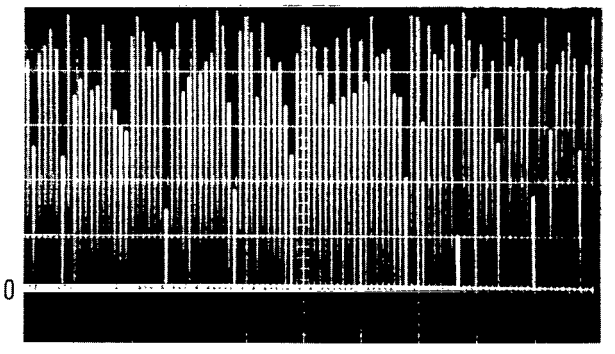

(e) Engine speed, 2140 rpm; torque, 119 J (88 ft-lb); equivalence ratio, 0.77; mean, 281 997 Pa (40.9 psi); standard deviation, 61 364 Pa (8.9 psi).

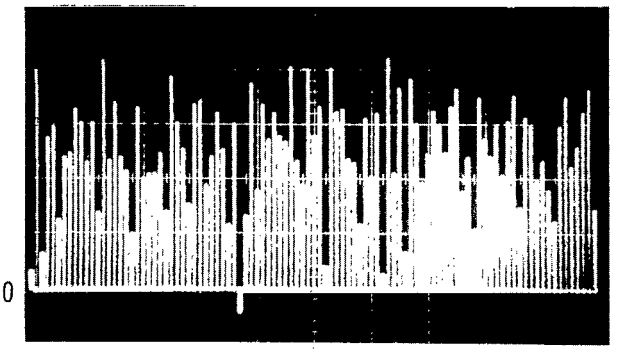

(f) Lean limit; equivalence ratio, 0.66; mean, 175 128 Pa (25.4 psi); standard deviation, 67 362 Pa (9.77 psi).

Figure 5. - Bar graphs of indicated mean effective pressure as function of equivalence ratio.

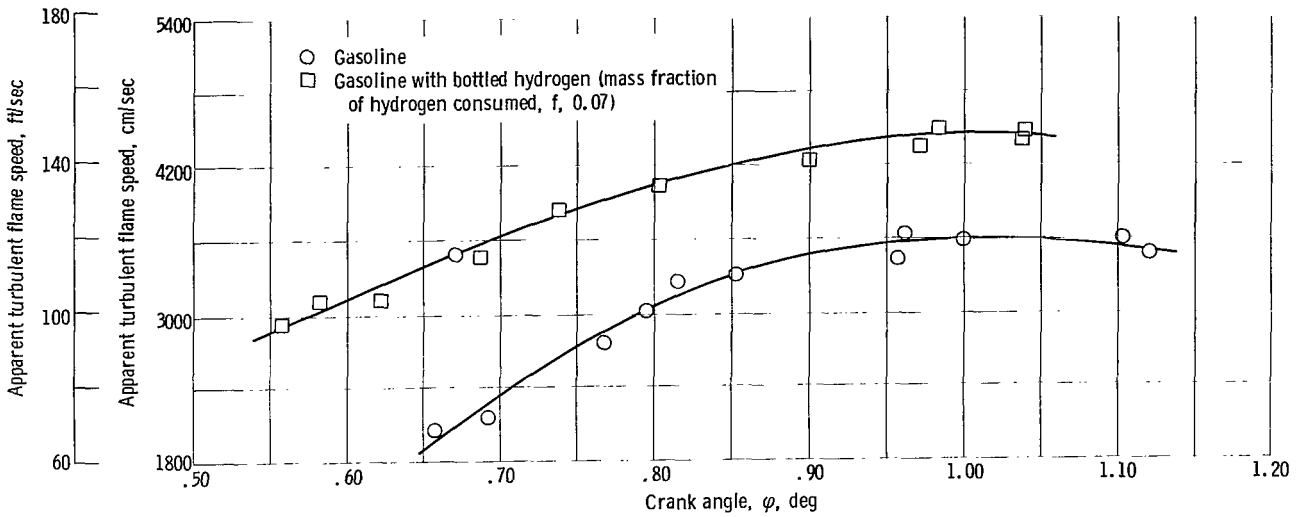

Figure 6. - Apparent turbulent flame speed as function of equivalence ratio. Engine speed, 2140 rpm; brake horsepower, 27 kW (36 bhp).

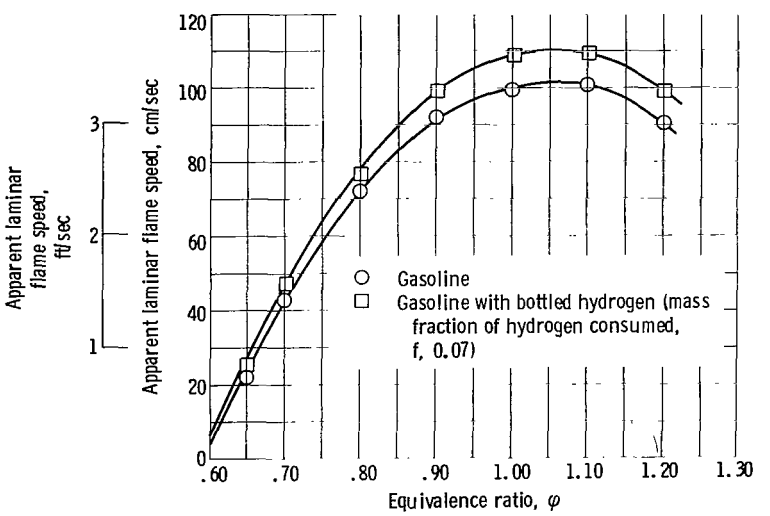

Figure 7. - Apparent laminar flame speed as function of equivalence ratio. Initial temperature, 600 K (620° F); initial pressure, 962 887 Pa (140 psi).

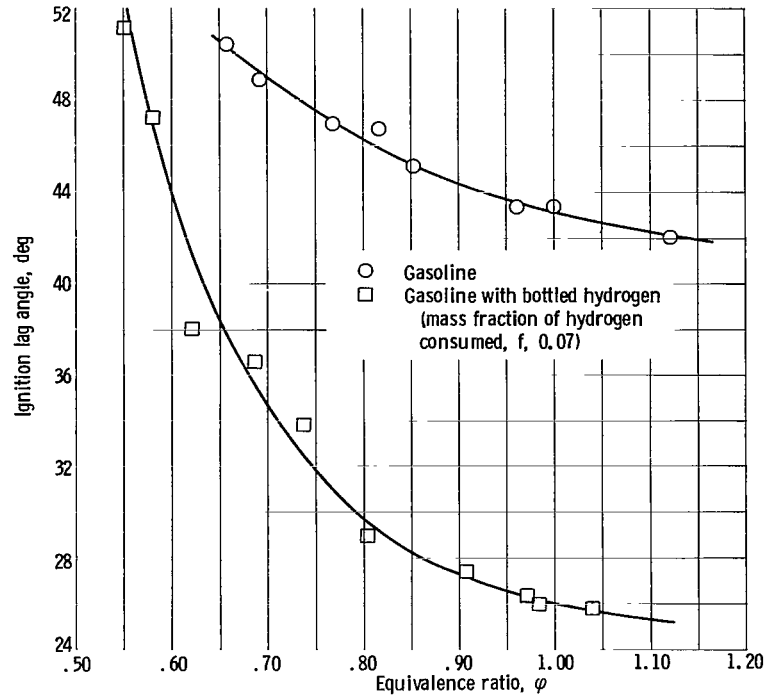

Figure 8. - Ignition lag angle as function of equivalence ratio. Engine speed, 2140 rpm; brake horsepower, 27 kW (36 bhp).

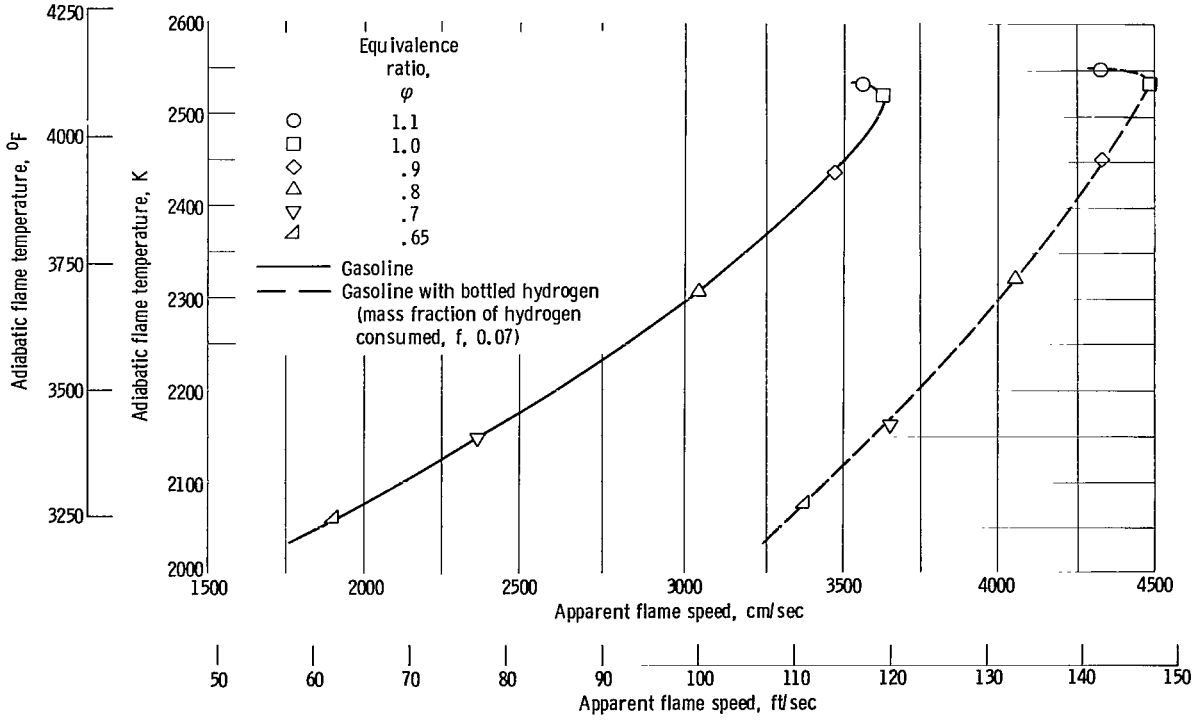

Figure 9. - Adiabatic flame temperature as function of apparent flame speed. Initial temperature, 600 K (620° F); initial pressure, 962 887 Pa (140 psi).

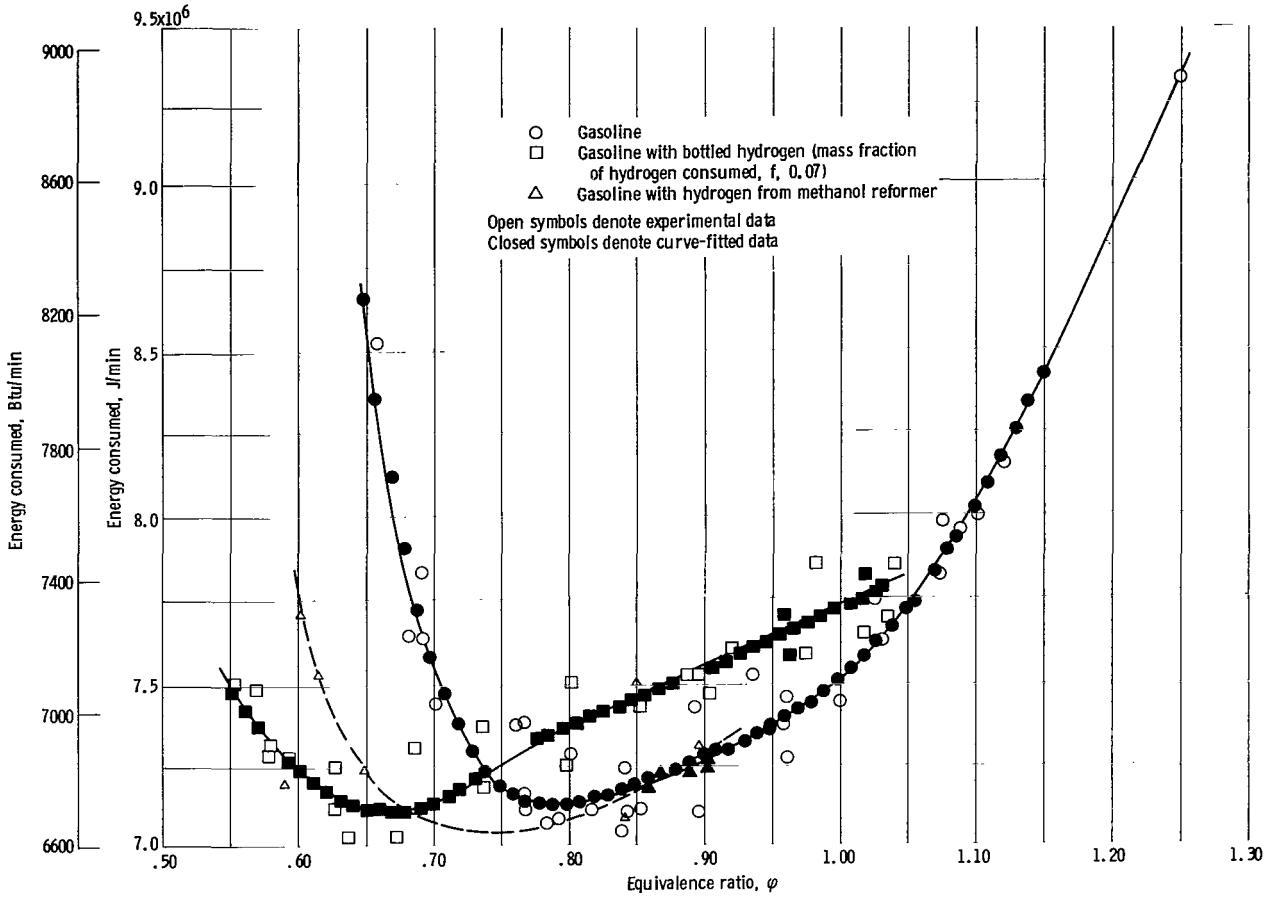

Figure 10. - Energy consumption as function of equivalence ratio. Engine speed, 2140 rpm; brake horsepower, 27 kW (36 bhp).

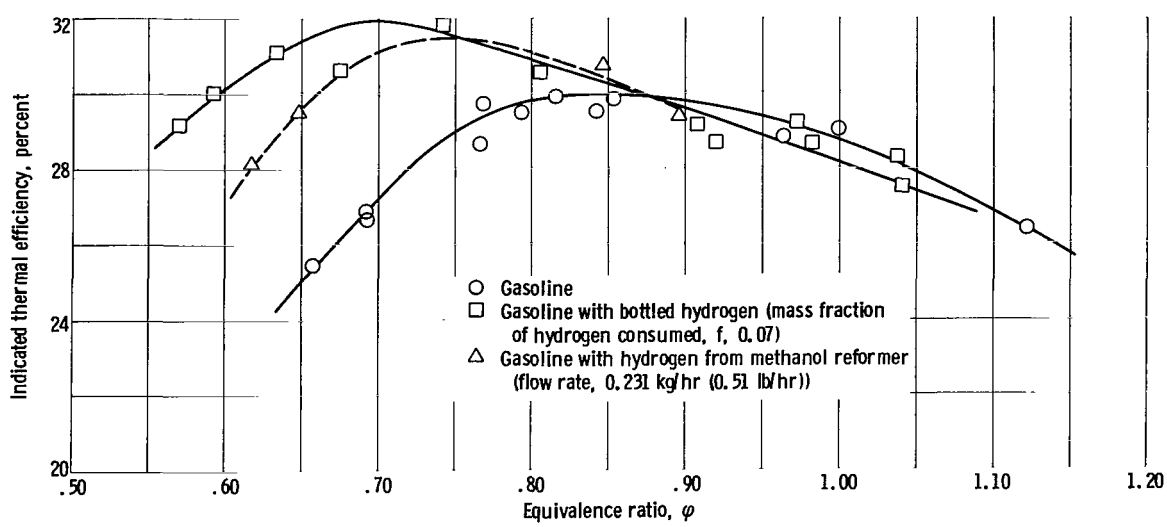

Figure 11. - Indicated thermal efficiency as function of equivalence ratio. Engine speed, 2140 rpm; brake horsepower, 27 kW (36 bhp).

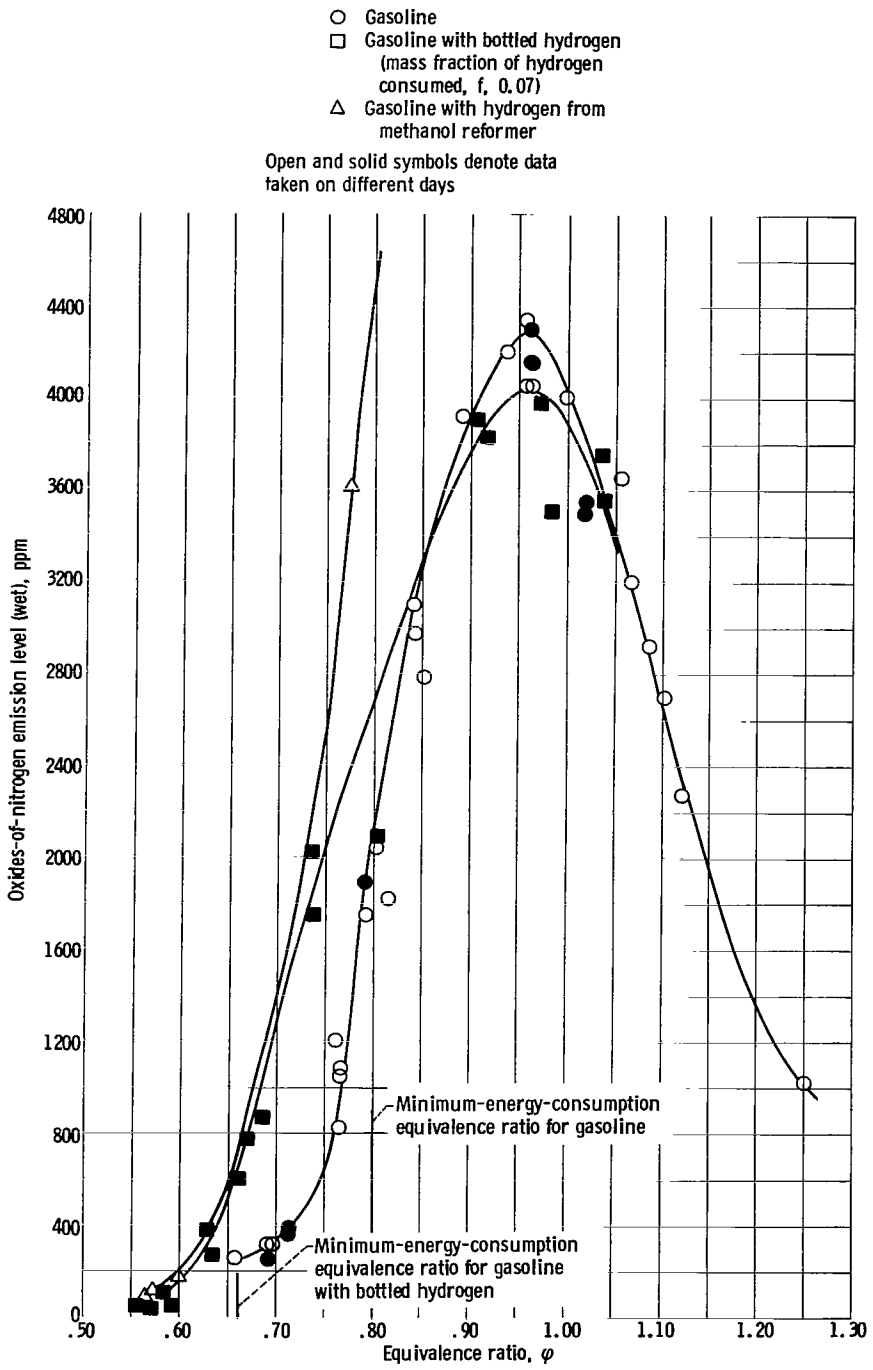

Figure 12. - Oxides-of-nitrogen emission level as function of equivalence ratio. Engine speed, 2140 rpm; brake horsepower, 27 kW (36 bhp).

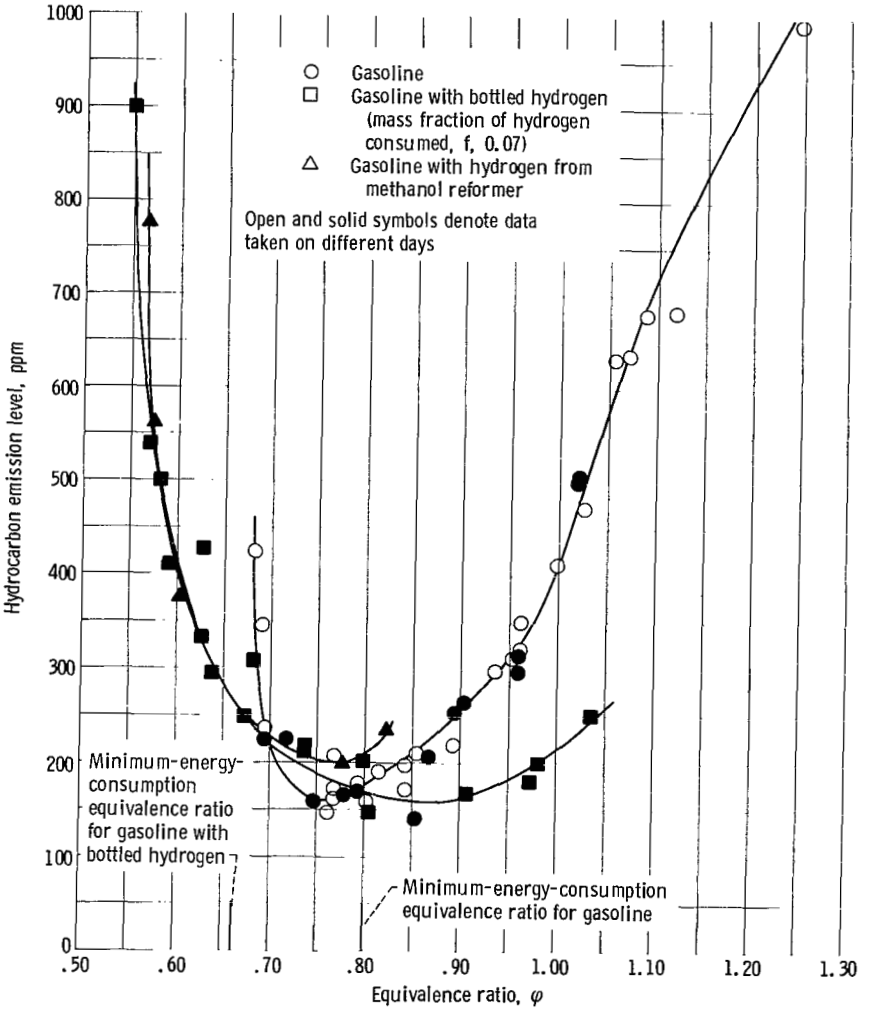

Figure 13. - Hydrocarbon emission level as function of equivalence ratio. Engine speed, 2140 rpm; brake horsepower, 27 kW (36 bhp).

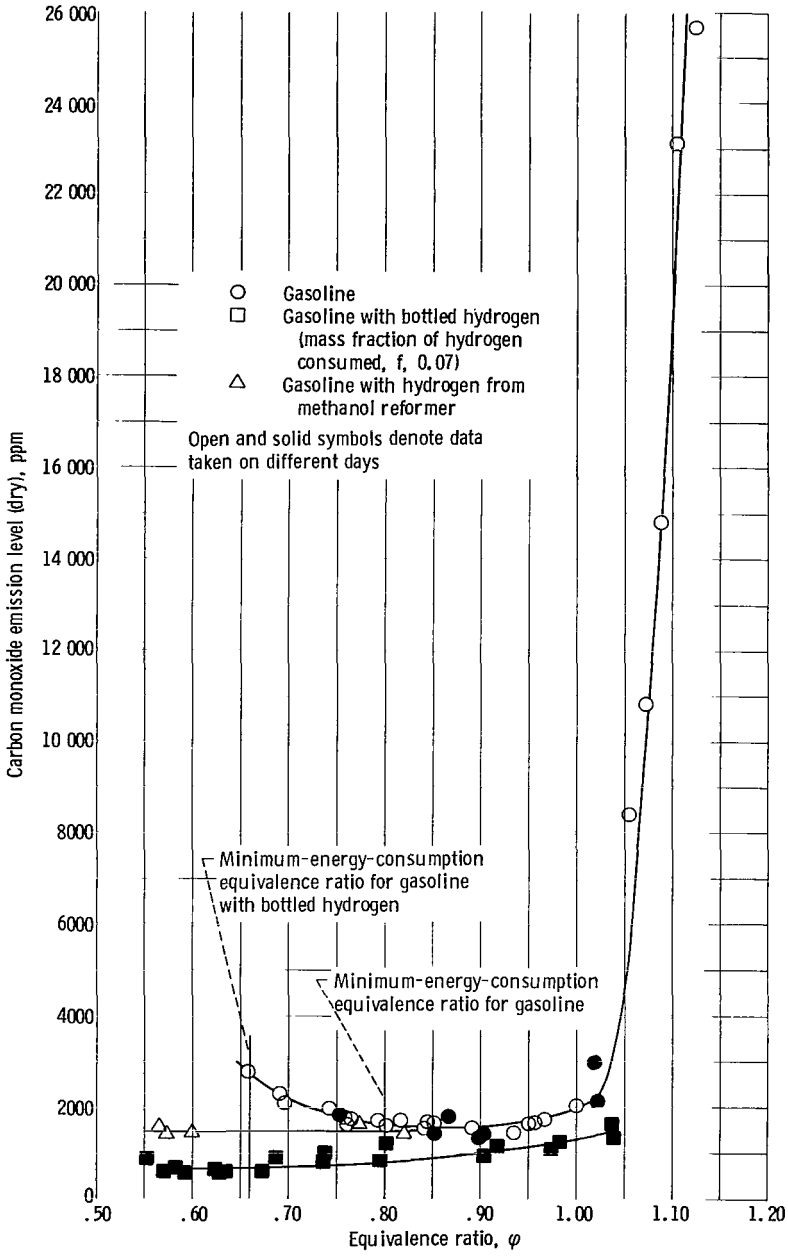

Figure 14. - Carbon monoxide emission level as function of equivalence ratio. Engine speed, 2140 rpm; brake horsepower, 27 kW (36 bhp).

"The aeronautical and space activities of the United States shall be conducted so as to contribute . . . to the expansion of human knowledge of phenomena in the atmosphere and space. The Administration shall provide for the widest practicable and appropriate dissemination of information concerning its activities and the results thereof."

—NATIONAL AERONAUTICS AND SPACE ACT OF 1958

NASA SCIENTIFIC AND TECHNICAL PUBLICATIONS

TECHNICAL REPORTS: Scientific and technical information considered important, complete, and a lasting contribution to existing knowledge.

TECHNICAL NOTES: Information less broad in scope but nevertheless of importance as a contribution to existing knowledge.

TECHNICAL MEMORANDUMS: Information receiving limited distribution because of preliminary data, security classification, or other reasons. Also includes conference proceedings with either limited or unlimited distribution.

CONTRACTOR REPORTS: Scientific and technical information generated under a NASA contract or grant and considered an important contribution to existing knowledge.

TECHNICAL TRANSLATIONS: Information published in a foreign language considered to merit NASA distribution in English.

SPECIAL PUBLICATIONS: Information derived from or of value to NASA activities. Publications include final reports of major projects, monographs, data compilations, handbooks, sourcebooks, and special bibliographies.

TECHNOLOGY UTILIZATION PUBLICATIONS: Information on technology used by NASA that may be of particular interest in commercial and other non-aerospace applications. Publications include Tech Briefs, Technology Utilization Reports and Technology Surveys.

Details on the availability of these publications may be obtained from:

SCIENTIFIC AND TECHNICAL INFORMATION OFFICE

NATIONAL AERONAUTICS AND SPACE ADMINISTRATION

Washington, D.C. 20546